The dynamic and static mechanical characteristics of Sn-7Zn-based solder alloy modified with microalloying of In, Fe and Co elements

I. H. Lotfy[1,*], S. A. Mansour[1], and A. M. El-Taher[2]

[1] *Physics Department, Faculty of Science, Suez Canal University, Ismailia, Egypt*
[2] *Physics Department, Faculty of Science, Zagazig University, Zagazig, Egypt*

Received: 9 July 2022
Accepted: 11 October 2022
Published online: 1 November 2022

© The Author(s) 2022, corrected publication 2023

ABSTRACT

Tensile creep experiments and pulse-echo overlap (PEO) method were utilized to analyze the impact of small additions of 2.5%wt In, Fe and Co (0.1%wt for each) on the creep resistance and elastic properties of a cast Sn-7Zn alloy. The In-modified alloy displays noticeably enhanced creep resistance and increased the fracture time ($\sim$ 2.7 times) due to precipitation strengthening and formation of γ-$InSn_4$ particles. The In-modified alloy exhibits an as-solidified grain structure, which is finer than the Sn-7Zn alloy, and predicted to enhance deformation resistance by lattice self-diffusion creep. Nonetheless, the creep resistance of Sn-7Zn alloy deteriorates after Fe and Co addition, highlighting the excellent coarsening of the new γ-$Zn_{21}Co_5$, γ-Co_2Sn_2Zn, and α-$Fe_{0.92}Sn_{0.08}$ precipitates. The obtained results implied that the creep strain rate follows the Garofalo hyperbolic sine equation, and the computed creep stress exponent is consistent with a climb-controlled dislocation creep. Consequently, for all PEO tests, the values of resulting Young's modulus (E) (66.7 GPa) and shear modulus (G) (20.5 GPa) of In-modified Sn-7Zn alloy were superior to those of the conventional plain Sn-7Zn alloy and Fe and Co modified alloy in its cast condition.

1 Prime Novelty Statement

The prime goal of this study is to assess the influence of In, Fe, and Co microalloying on the microstructure, creep characteristics, "plastic deformation" and elastic behavior of the Sn-7Zn alloy. The investigations revealed that 2.5%wt addition of In microalloying causes a notable change in the Sn-7Zn microstructure by eliminating the undesirable needle-like Zn particles, refining the β-Sn grains, and the formation of a new γ -InSn4 IMC. These changes are reflected in the mechanical behavior of the ternary Sn-7Zn-2.5In solder, since it can result in evading the strength-ductility trade-off phenomena, which is a major concern in the electronic industry. Conversely, 0.1%wt addition of Fe and Co leads to the formation of many coarsening γ-Zn21Co5, γ-Co2Sn2Zn, and α-Fe 0.92Sn 0.08 IMCs that enhance the ductility of the

Address correspondence to E-mail: Islamhamada24@gmail.com

https://doi.org/10.1007/s10854-022-09340-0

sample but at the expense of its strength. Furthermore, the pulse-echo overlap (PEO) tests come with an outstanding finding that the formation of IMCs regulates the elastic properties of the tested solders. The finding revealed that the presence of coarse IMCs in the quaternary alloy leads to a larger Poisson's ratio of 0.38, a greater attenuation coefficient of 731.19 dB/m, and a higher bulk modulus of 83GPa, indicating that it has higher ductility, a shorter resonant life, and high compressibility, respectively.

2 Introduction

Global reservations over using lead in solder alloys are a pressing problem for the electronic industry. Consequently, various lead-free solder systems are being intensively investigated and chosen as potential replacements for Sn-Pb solder [1]. Sn-Zn solder alloy systems are nominated as excellent alternatives to Sn-Pb solders because of their inexpensive cost, suitable melting temperature, and outstanding mechanical qualities. However, Zn is an active material with a tendency to corrode, in addition to the poor oxidation resistance and wetting qualities of the Sn-Zn systems restricting the use of Sn-Zn alloys as essential components of electronic devices [2–4]. Two possible approaches have been suggested to solve this challenge. First, it has been shown that the microstructural mechanism that makes solder joints more reliable is set off by the formation of a second phase, which could be achieved by doping Sn-Zn solder with various alloying materials like Ag, Ni, Bi, In, Co, and Ga [2]. Second, corresponding to the binary Sn-Zn phase diagram illustrated in Fig. 1 [5], lowering the Zn quantity within the Sn-Zn alloys can restrict its adverse impact while preserving the eutectic melting point. This is because the tendency of the liquidus curve at the hypo-eutectic area is not very high. Hence, decreasing Zn percent around Sn–9Zn would not lead to a significant rise in the equilibrium liquidus temperature, implying that the higher cost of lead-free solders is, the less oxidation sensitivity of Zn would be [6]. For example, according to Yanzhi Peng et al. [7], microalloying Sn-9Zn-2Bi solder alloy with Ga resulted in: (1) removing the coarse Zn-rich phase; (2) vanishing of intermetallic compounds (IMC) as a result of Ga's complete solubility in Zn; (3) enhancing the wettability of the Sn–9Zn–2Bi alloy; (4) increasing the resistance of the system; (5) increasing the ultimate tensile strength of the material; (6) diverting the fracture into a mixed rupture rather than a nearly completely ductile fracture; and (7) effectively preventing further corrosion, particularly when the Ga concentration is increased to 0.3wt%.

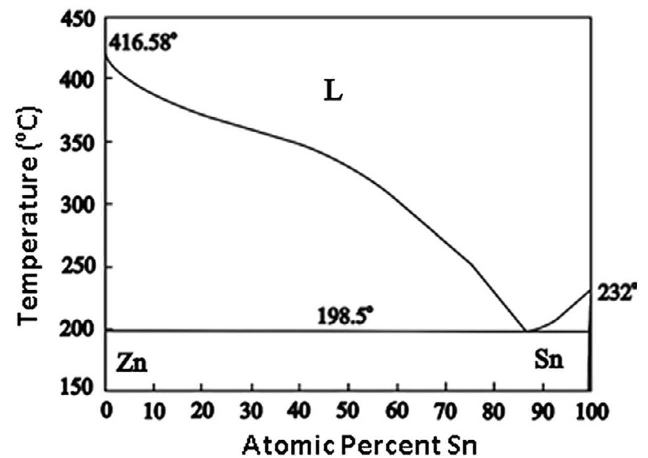

Fig. 1 Binary Sn–Zn phase diagram [5]

Furthermore, Mahmudi et al. [8] studied Bi impact on the creep characteristics owned to the Sn-9Zn solder where they observed that the ternary alloy improves creep resistance because of the solid solution impact and precipitation of Bi in the Sn matrix. Wei et al. [5] assessed the non-equilibrium melting and wetting properties of a variety of Sn-xZn alloys where x represents the %wt Zn concentration and varied from 2.5% to 9%. They stated that although Sn-6.5Zn melts similarly to eutectic Sn-9Zn, it has considerably higher wettability to Cu compared to Sn-9Zn. Therefore, Sn-6.5Zn would be preferable to Sn-9Zn. Tikale et al. [9] demonstrated that lowering the Zn content lowers the thickness of the filler metal's IMC. The objective of this research is to assess the impact of the addition of minimal amounts of In, Fe, and Co on the microstructure, creep characteristics, plastic deformation of the hypo-eutectic Sn–7Zn solder in addition to its elastic behavior. The essential parameters that determine the microstructure, creep characteristics, plastic deformation and elastic behavior of the investigated alloys are described. It is hypothesized that these minor element additions should help improve the overall microstructure, creep characteristics, plastic deformation, and elastic behavior of the investigated alloys. The obtained data are expected to help make new solder alloys for use in various kinds of electronic packaging.

3 Experimental procedures

3.1 Sample preparations

In this study, the metal ingots were blended to form binary Sn-7wt%Zn, ternary Sn-7wt%Zn-2.5wt%In, and quaternary Sn-7wt%Zn-0.1wt%Fe-0.1wt%Co solder alloys. The melting procedure was accomplished via mixing the alloy elements in a quartz tube that was inserted in an electric furnace at 600 °C for around 1 h in a KCl + LiCl (1.3:1) environment. A graphite rod was used to stir the molten metal mechanically so that the prime alloy would dissolute. Then, the samples were cast into a steel mold and allowed to cool at a rate of 6–8 °C/s to assemble microstructures like those found in small solder junctions in the electronics industry. The surfaces of the obtained alloy specimens in polished and etched conditions were inspected using optical microscopy (OM) (OM, KEYENCE VHX-500F) and scanning electron microscope (SEM) (quanta feg 250, made in – republic Czech). Nonetheless, an X-ray diffractometer (XRD) (PHILIPS X'Pert Diffractometer) at 40 kV and 20 mA using CuKα rays with a diffraction angle (2θ) ranging 25° to 100° and a steady scanner velocity of 1°/min was used to figure out the phase of the alloy specimens. The alloy specimens were divided into two groups. The first group was shaped as a wire specimen having a length of 4×10^{-2} m and a diameter of 1.2×10^{-3} m. This group was annealed at 120 °C for 1 h to minimize remaining tension acquired during the specimen preparation and then allowed to cool gently to ambient temperature before microstructure study, and mechanical tests. The mechanical evaluations were carried out by utilizing an Instron type machine with experimental errors less than ± 3%. The tensile creep tests were performed at temperature range of 25–120 °C, and different constant loads. Tensile creep tests are accomplished using ASTM E8/E8M-13a standard test methods for tension testing of metallic materials. The temperature of furnace was automatic controlled with ± 1 °C. The loading process is controlled, and the experimental data are recorded by a computer system [10].

3.2 Ultrasonic velocity measurements

The PEO approach, represented in Fig. 2, is a non-damaging technique applied to assess the mechanical wave velocity in alloy samples. The specimens were refined with 5×10^{-4} m Al_2O_3 particles. The surface alignment between the opposite sides was assessed with a surface plate with a ± 25 m accuracy. The ultrasonic velocities were evaluated utilizing the criteria of electronic circuit (Hewlett Packard 54,615 B) by estimating the time interval between the initiating pulse and the receiving pulse displayed on a flaw detector's monitor (USIP20-Kraütkramer). Since velocity is defined as the distance covered by an item divided by the time it takes to travel that distance, the wave velocity can be computed using the equation $\upsilon = 2x/\Delta t$, where (x) is the specimen thickness and (Δt) is the time interval [11, 12]. Both longitudinal (v_l) and shear ultrasonic (v_s) wave velocities were recorded at room temperature using the Karl Deutsch transducer S12 HB4 and the Kraütkramer transducer K4KY with a fundamental frequency of 4 MHz. The propagation velocity of ultrasonic waves was assessed by high accuracy of ± 13 m/s for v_l and ± 8 m/s for v_s. It was noticed that the material's nature controls the magnitude of both v_l and v_s wave velocities. The density of each alloy specimen can be calculated using Archimedes' principle. In this investigation, the density of the specimen was assessed at room temperature (25 °C) by employing toluene as an immersion fluid and using the next equation:

$$\rho = \rho_b \frac{w_a}{w_a - w_b} \tag{1}$$

whereas (ρ_b) is the density of the buoyant and (w_a) and (w_b) are the sample weights in air and the buoyant, respectively.

Errors in the density calculations of the investigated specimens were reduced up to ± 5 kg/m^3 by repeating each experiment several times. Elastic coefficients such as Young's modulus (E), shear modulus (G), bulk modulus (K), and Poisson's ratio (υ) were estimated via this investigation. According to El-Daly and Hammad et al. [2], υ is assessed to deliver additional data on the nature of bonding forces than other elastic coefficients where υ correlates with E and G through the relation:

$$\upsilon = \frac{E}{2G} - 1 \tag{2}$$

Furthermore, υ correlates with v_l and v_s through the relation:

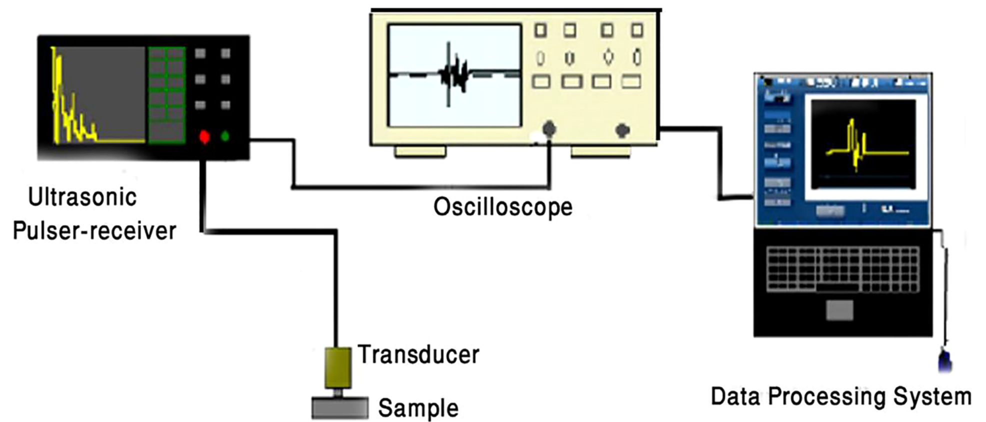

Fig. 2 Schematic representation of pulse-echo overlaps (PEO) method [11]

$$\upsilon = \frac{v_i^2 - 2v_s^2}{2(\mathrm{Vl}^2 - \mathrm{Vs}^2)} \quad (3)$$

In addition, v_l and v_s correlate with E and G through the relation:

$$E = \frac{3\rho v_s^2\left[v_l^2 - \left(\frac{3}{4}\right)v_s^2\right]}{\left(v_l^2 - v_s^2\right)} \quad (4)$$

$$G = \rho v_s^2 \quad (5)$$

$$K = \frac{E}{3(1 - 2\upsilon)} \quad (6)$$

$$\mathrm{G} = \frac{E}{2(1 + \upsilon)} \quad (7)$$

The following equation could be used to determine both the attenuation coefficients (α) and hardness (H):

$$\alpha = 20\frac{\mathrm{Log}\left(\frac{\mathrm{Ai}}{\mathrm{Aj}}\right)}{2X} \quad (8)$$

$$H = \frac{E(1 - 2\upsilon)}{6(1 + \upsilon)} \quad (9)$$

whereas (A_i) and (A_j) are the echo heights of consecutive peaks i and j, respectively.

4 Discussion of the findings

4.1 Microstructure examination

The morphological changes caused by the additions of 2.5wt% In, 0.1wt% Fe, and 0.1%wt Co into the binary Sn-7Zn solder alloy were analyzed using OM and SEM; the obtained results are depicted in Figs. 3–5. The results revealed that the Sn-7Zn alloy micrograph is characterized by the presence of needle-forms of α-Zn that are widely spread within the β-Sn matrix, Figs. 3A, 4A and 5A. The 2.5%wt In addition to the Sn-7Zn alloy leads to a refinement of the needle-forms of α-Zn in the β-Sn matrix in addition to the formation of new IMC, Figs. 3B, 4B and 5B. Furthermore, the doping 0.1%wt Fe and Co to the Sn-7Zn solder alloy leads to the suppression of Zn needle structures in addition to the production of coarse-butterfly shapes, Figs. 3C, 4C and 5C. Furthermore, XRD technique was used to recognize the initial phases of the as-solidified alloys. The results obtained, illustrated in Fig. 6a–c, revealed that the Sn-7Zn alloy morphology contains β-Sn and α-Zn-rich phases without any sign of IMCs formation. This is due to the low solubility of Zn in Sn back to Sn-Zn binary phase diagram, shown in Fig. 1 [5]. With doping In into the binary Sn-7Zn alloy, the ternary alloy morphology contains three phases of β-Sn, α-Zn and the new γ-$InSn_4$ IMC, which implies that In has a complete solubility in the Sn matrix [13]. Nevertheless, a massive change in the morphology of Sn-7Zn solder alloy had been observed after the addition of Fe and Co, where the XRD analysis for the quaternary alloy reveals the presence of β-Sn, α-Zn, α-Fe, γ-$Zn_{21}Co_5$, γ-Co_2Sn_2Zn, and α-$Fe_{0.92}Sn_{0.08}$. Similar results were obtained by Giefers and Nicol [14], Shou-li et al. [15], and Abou-krisha and Abushoffa [16].

4.2 Tensile creep properties

4.2.1 Alloy properties

In this study, to obtain the creep curves, the specimens were subjected to stresses ranging from 23.40 to

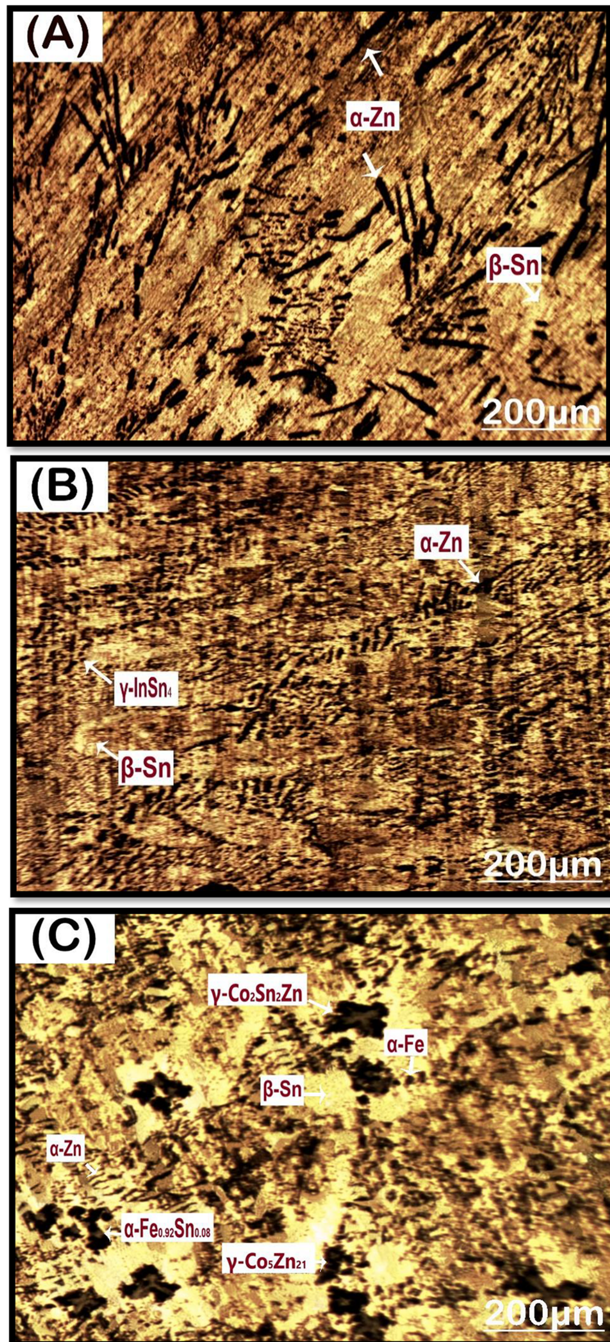

Fig. 3 OM microstructures of solidified **A** Sn-7Zn, **B** Sn-7Zn-2.5In and **C** Sn-7Zn-0.1Fe-0.1Co alloys

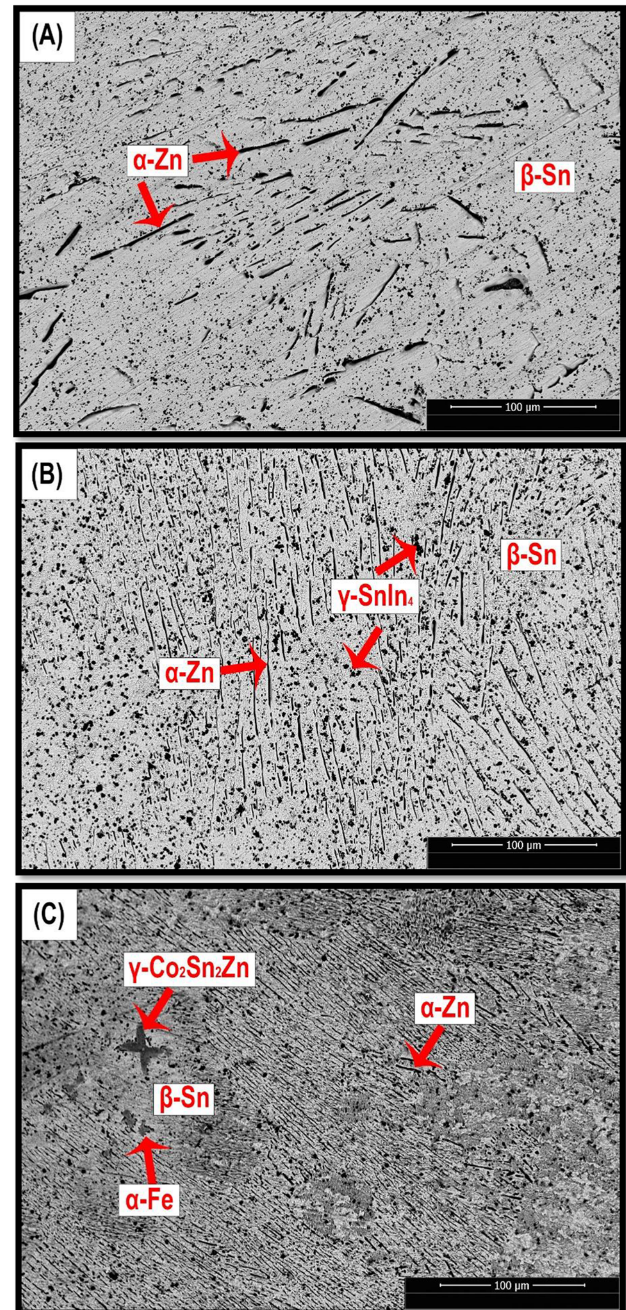

Fig. 4 Low-magnification SEM image of **A** Sn-7Zn, **B** Sn-7Zn-2.5In and **C** Sn-7Zn-0.1Fe-0.1Co solder alloys

31.39 MPa at ambient temperature; the findings are shown in Fig. 7. The produced creep curve has a conventional form with well-defined creep characteristics creating an evident transition across the primary, secondary, and tertiary creep phases throughout the time interval studied. The results showed that adding 2.5In to the binary Sn-7Zn reduces the creep rates and improves the creep resistance, whereas adding 0.1Fe and 0.1Co to the binary Sn-7Zn increases the creep rates and, hence, decreases the creep resistance. The creep-rupture tests were studied at 25, 50, 70, 90, and 120 °C, respectively, under the influence of constant stress of 23.40 MPa, and the model forms of strain (%) vs. time curves for the investigated alloys, illustrated in Fig. 8.

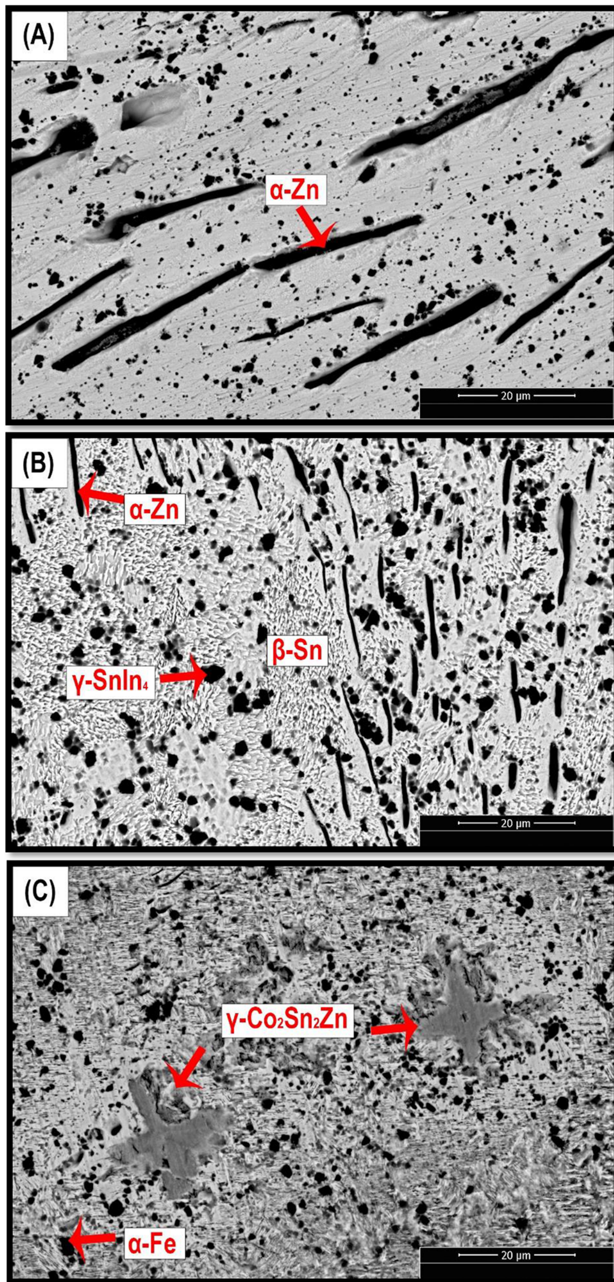

Fig. 5 High-magnification SEM image of **A** Sn-7Zn, **B** Sn-7Zn-2.5In and **C** Sn-7Zn-0.1Fe-0.1Co solder alloys

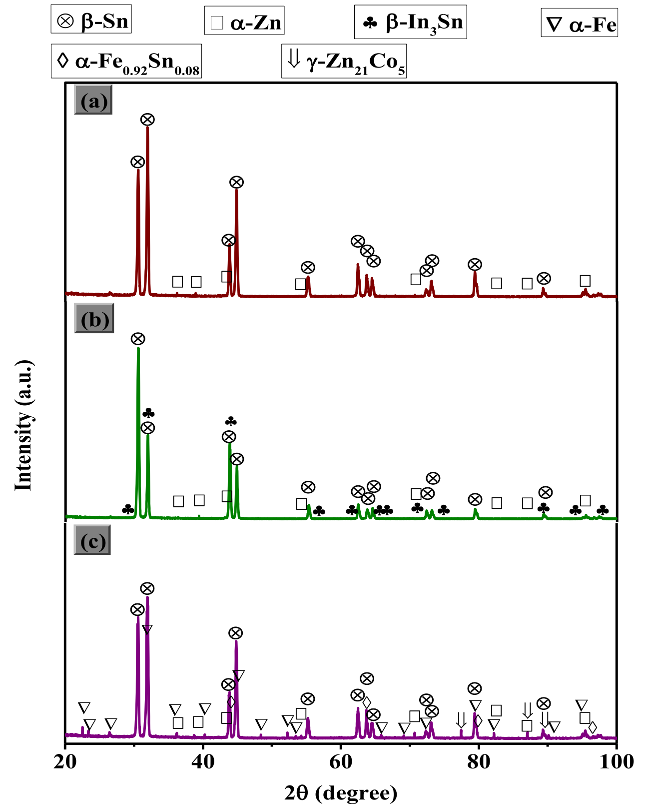

Fig. 6 XRD analysis of as-solidified **a** Sn–7Zn, **b** Sn–7Zn–2.5In and **c** Sn–7Zn–0.1Fe-0.1Co solder alloys.

It is worth noting that the addition of 2.5In to the binary Sn-7Zn decreases the creep rates, whereas the addition of 0.1Fe and 0.1Co to the binary Sn-7Zn increases the creep rates. Furthermore, the creep curve trend demonstrates a rapid transition from brief primary creep to well-defined steady-state creep, indicating that the matrix hardening caused by the creep strain was quickly retrieved and balanced at the prolonged deformation rate. The creep resistance of the complete alloy samples can be compared using the plot of the computed creep rates (ε) of the three solders as a function of time in Fig. 9.

When compared to the other two alloys, the Sn-7Zn-2.5In alloy had a significantly lower steady-state creep rate and roughly larger fracture times (2.7 times) than the binary Sn-7Zn. These results confirmed that 2.5In enhances both ductility and strength compared to the base Sn-7Zn solder alloy, so that Sn-7Zn-2.5In solder alloy is known as a visco-plastic solder alloy, which is a favorable property needed in electronic packaging. In addition, the size, shape, and amount of γ-$InSn_4$ IMC particles may improve the visco-plastic deformation resistance of the solder and constrain the microstructure evolution caused by dislocation movement. Such movement could explain why the ternary Sn-7Zn-2.5In becomes a visco-plastic material. Nonetheless, the coarse IMCs γ-$Zn_{21}Co_5$, γ-Co_2Sn_2Zn, and α-$Fe_{0.92}Sn_{0.08}$ created by the inclusion of 0.1Fe and 0.1Co into the Sn-7Zn alloy are easily fractured reducing the strength effects of the quaternary Sn-7Zn-0.1Fe-0.1Co solder [17]. Figure 10 shows SEM of the fracture surfaces of the tensile

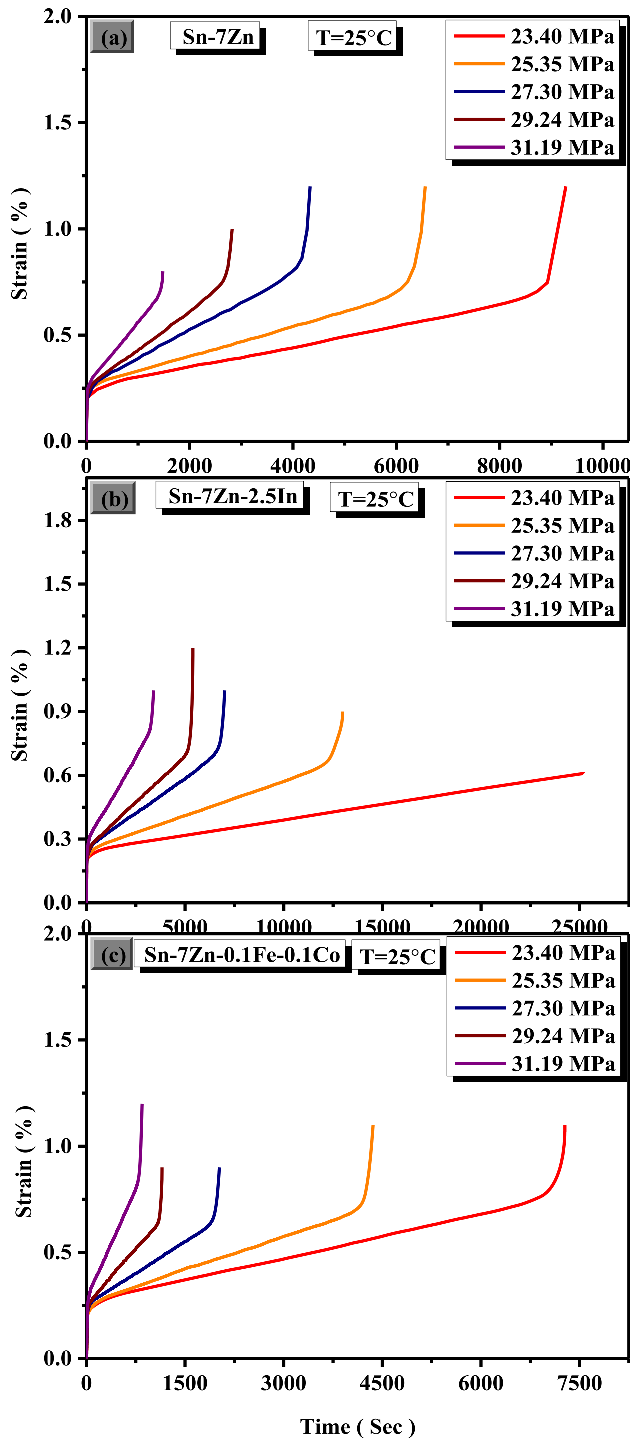

Fig. 7 Representative creep curves for the **a** Sn-7Zn, **b** Sn-7Zn-2.5In and **c** Sn-7Zn-0.1Fe-0.1Co solder alloys tested at room temperature T = 25 °C and under different stresses as indicated

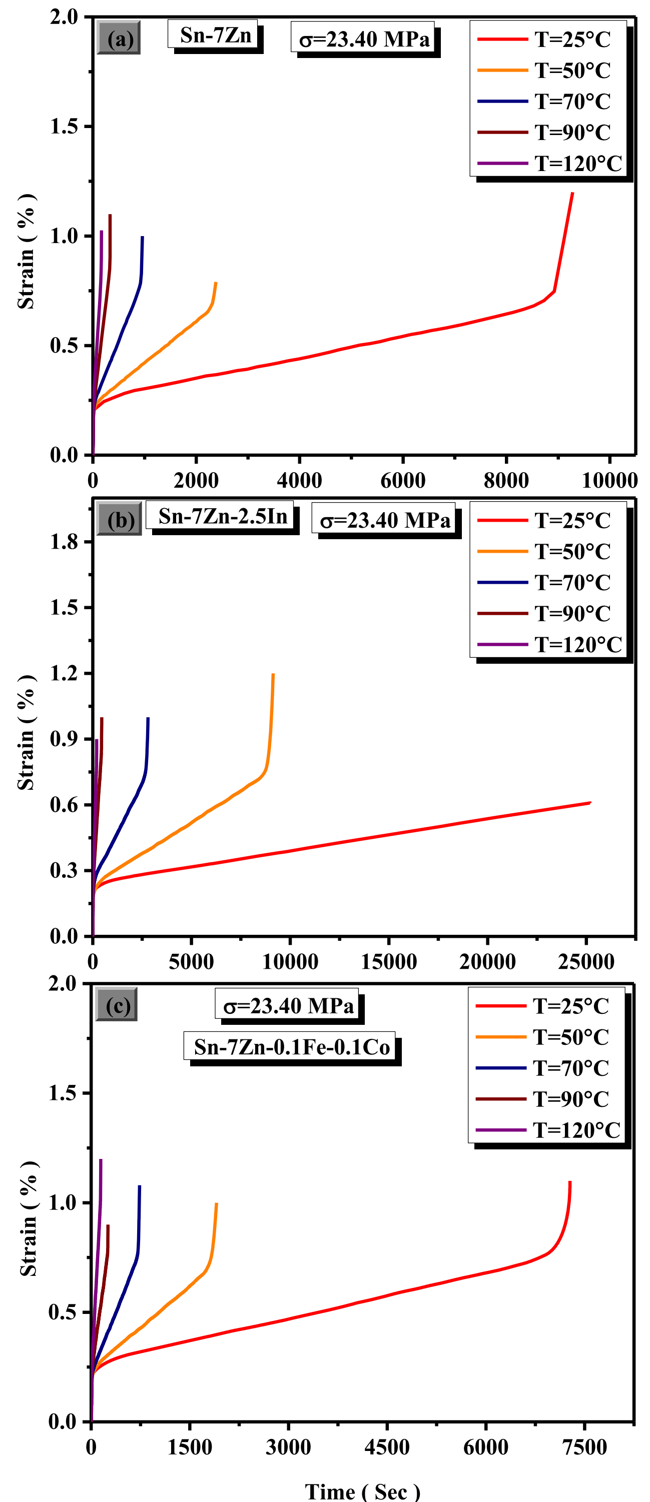

Fig. 8 Variation of Creep curves at different temperatures and constant stress of 23.40 MPa for **a** Sn-7Zn, **b** Sn-7Zn-2.5In and **c** Sn-7Zn- 0.1Fe-0.1Co solder alloys

creep specimens for Sn-7Zn, Sn-7Zn2.5In and Sn-7Zn-0.1Fe-0.1Co solder alloys. A ductile dimple pattern can be seen at all solder alloys. It was found that an additional 2.5In wt.%, small-sized cup and cone fracture obtained. This indicates a reduction in the ductility indicating a higher creep resistance.

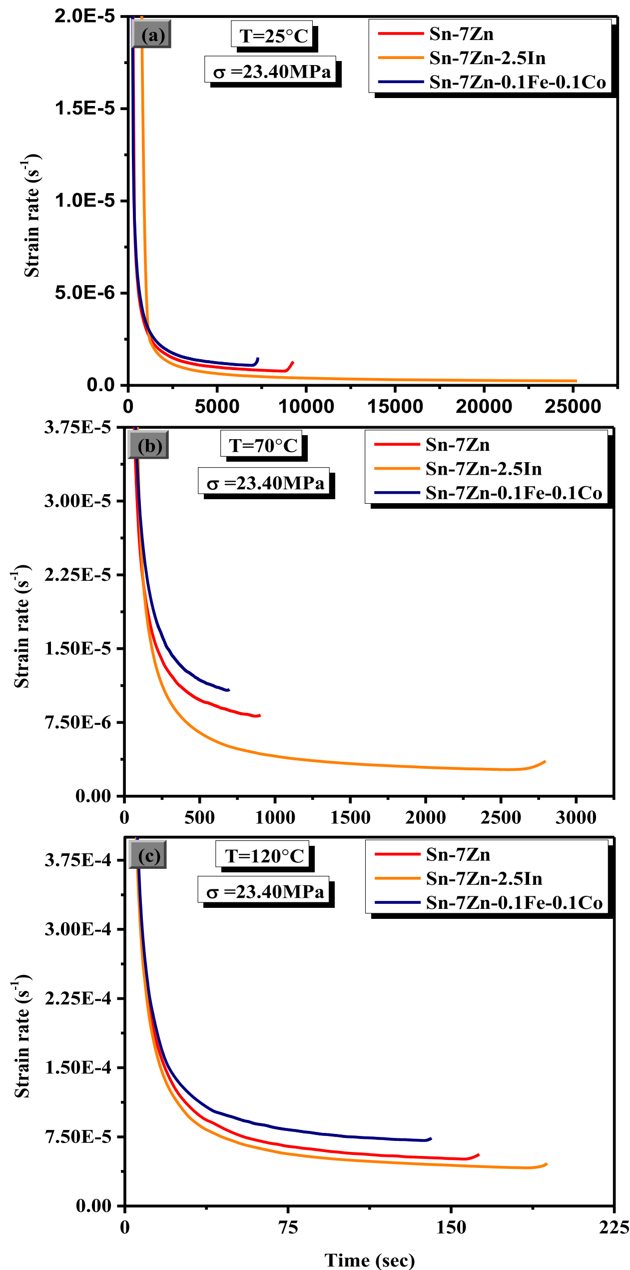

Fig. 9 Comparison of creep curves, Strain rate and time curves at T = 25 °C, T = 50 °C, T = 70 °C, T = 90 °C and T = 120 °C and σ = 23.40 MPa for **a** Sn-7Zn, **b** Sn-7Zn-2.5In and **c** Sn-7Zn-0.1Fe-0.1Co solder alloys

However, with the addition of a 0.1 wt.% Fe and 0.1wt.% Co, the size of the cup and cone fracture becomes larger. This indicates an increase in the ductility indicating a lower creep resistance. These findings are consistent with creep curves results in Fig. 7. As for the microstructure analyses, it can be noticed that the mechanical characteristics of the Sn-7Zn solders were governed by the distribution of the needle-form α-Zn phases in the β-Sn matrix. Therefore, the formation of γ-$InSn_4$ IMCs and finely scattered needle-form α-Zn phases in the entire β-Sn matrix impedes the dislocation movement. Consequently, the creep resistance of the specimen is dramatically enhanced, which could be responsible for the increased creep resistance of Sn-7Zn-2.5In.

4.2.2 Deformation solder kinetic analysis

One of the objectives of this research is to figure out the creep mechanism of Sn-7Zn alloy, which can be accomplished by defining a set of material parameters such as the stress exponent (n) and activation energy (Q) of the operative deformation procedure. Generally, there are two approaches to examining creep data:

1- A basic power law derived from theoretical dislocation movement treatments. However, the higher stress exponent values, greater than 7, observed from creep studies on precipitation reinforced alloys cannot be explained by these standard textbook models of creep [18].

$$\dot{\varepsilon} = A\sigma^{n}exp(-Q/RT) \quad (10)$$

2- The Garafalo hyperbolic sine can be used to mimic a variety of stress exponents found at various temperatures,

$$\dot{\varepsilon} = A[sinh(\alpha\sigma)]^{n}exp(-Q/RT) \quad (11)$$

In Eqs. 10 and 11, (A) and (α) are the material constants in s^{-1} and MPa^{-1}, respectively; (α) is the stress level parameter; (R) is the universal gas constant; (n) is the stress exponent constant related to strain rate; (T) is the thermodynamic deformation temperature in Kelvin; (σ) is the steady-state flow stress in MPa; and (Q) is the deformation activation energy in kJ/mol.

Applying the natural logarithmic conversion to both sides of Eq. (11), we get

$$\ln \dot{\varepsilon} = \ln A + n \ln[\sinh(\alpha\sigma)] - Q/RT \quad (12)$$

In Eq. 12, the stress reciprocal (α) is the point where the deformation of the material changes from power to exponential stress dependence.

The α-value can be computed using the formula α = β/n_1, where β and n_1 are the average slopes of ln (ε) versus (σ) and ln (ε) versus ln (σ) at constant temperature, respectively, as shown in Figs. 11, 12

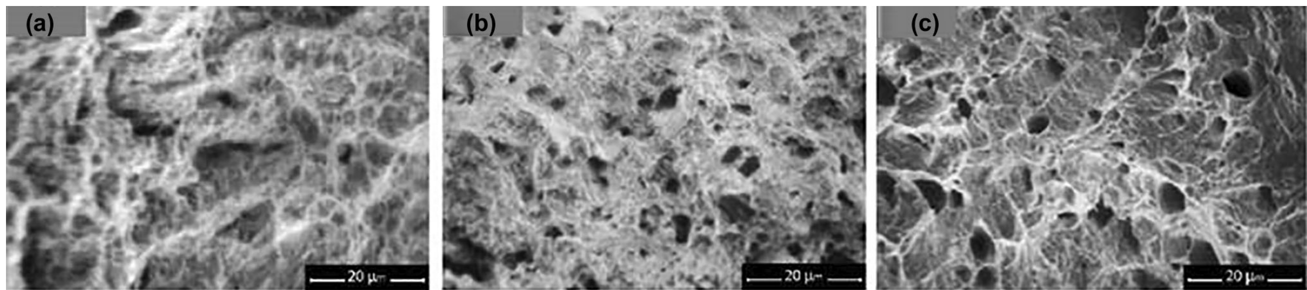

Fig. 10 SEM of the fracture surface of **a** Sn-7Zn, **b** Sn-7Zn-2.5In and **c** Sn-7Zn-0.1Fe-0.1Co solder alloys

and 13. The slope of the ln (ε) vs ln [sinh(ασ)] plot, shown in Figs. 11, 12 and 13, yielded the *n*-values, whereas the intercept of the ln (ε) against ln [sinh(ασ)] plot yielded the ln (A). The creep-activation energy Q values of the entire solder have been assessed using the linear retraction of the empirical data related to ln (ε) and 1/T, as shown in Fig. 14. Table 1 lists the parameters that were acquired. The findings revealed that different alloying additions result in different creep properties.

In this investigation, doping 2.5%wt In into Sn-7Zn solder alloy results in a lower creep rate and higher stress exponents (n = 5.01–6.3), while doping 0.1%wt Fe and 0.1%wt Co with Sn–7Zn results in an elevated creep rates and lowering the stress exponent (n = 4.28–5.48). This indicates that Fe and Co additions have a lower ability to strengthen the Sn-7Zn. Moreover, the fluctuation of n-values with temperature could be linked to the microstructure instability that can occur during high-temperature deformation. The results obtained in this investigation imply that the stress exponents of Sn-7Zn and Sn-7Zn-0.1Fe-0.1Co solders were nearly equal in this study because the prime phases were the base β-Sn. However, the higher stress n values of Sn-7Zn-2.5In could be due to the production of a significant amount of eutectic area because of the improved solid solution influence of In. Moreover, El-Daly and El-Taher [19] assumed that the variation in n-values of the investigated alloys suggests that the creep deformation is impacted by the formation of IMCs. Based on this assumption, it can estimate that the formation of γ-$InSn_4$ IMC due to the addition of In into the binary Sn-7Zn could obstruct dislocation climbing during creep by acting as dispersion strengtheners, resulting in *n*-values greater than 5, typical of precipitation-strengthened materials. Since driving forces are activated more slowly at low temperatures than at higher temperatures, the considerable increase in stress exponent values in the Sn-7Zn-2.5In alloy could imply that the interaction between dislocations and big eutectic particles has changed. This finding is plausible when the results from Fig. 3 are considered since the size and number of precipitates influence creep resistance. The creep behavior of the solder alloy is controlled by the phase producing a continued matrix, whether eutectic or base tin.

The activation energy results showed that the Sn-7Zn-2.5In alloy has a higher apparent activation energy of 77.4 kJ/mol, followed by 72.6 kJ/mol for Sn-7Zn and 67.1 kJ/mol for Sn-7Zn-0.1Fe-0.1Co indicating that the deformation mechanism for the ternary Sn-7Zn-2.5In is transformed from pipe to lattice self-diffusion mechanism, while both binary Sn-7Zn and quaternary Sn-7Zn-0.1Fe-0.1Co are controlled by a pipe diffusion mechanism [20]. The addition of In segregation to dislocation cores in the Sn-7Zn alloy would cause more local lattice distortions near the dislocation lines, increasing the deformation energy needed for such crystals. The differences between Q and n values and the other obtained data could be caused by several things, such as variations in applied techniques, microstructure, samples' preparation, errors in measurement process, and data handling methods.

4.3 Elastic properties "ultrasonic (US) examination"

Using the PEO method, the elastic coefficients for the three solder alloys, such as α, E, G, K, H, and υ, have been evaluated.

4.3.1 The effect of additives on ultrasonic velocities (V_l, V_s) and density

The empirical measurements of US wave velocities (V_l and V_s) and densities (ρ) of Sn-7Zn, Sn-7Zn-2.5In,

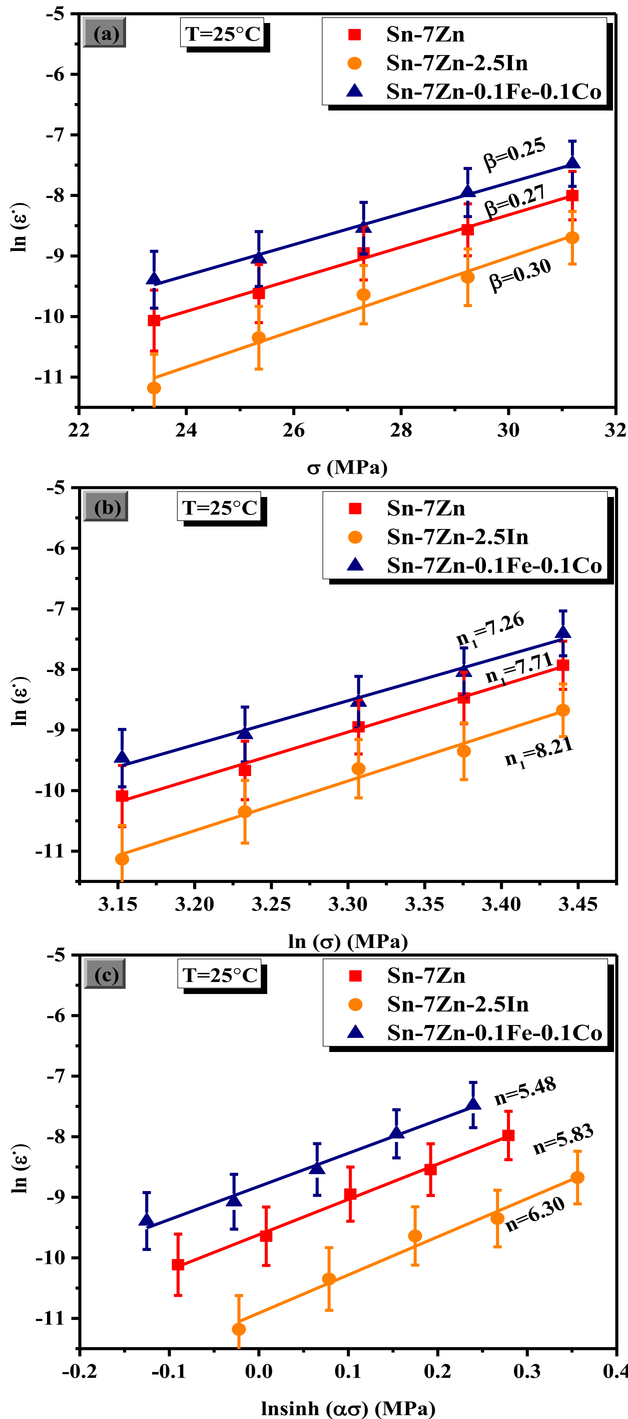

Fig. 11 Determination of β, n_1 and n from the slopes of $\ln \dot{\epsilon} - \sigma$, $\ln \dot{\epsilon} - \ln \sigma$ and $\ln \dot{\epsilon} - \ln [\sinh(\alpha\sigma)]$, respectively, at temperature of T = 25 °C for **a** Sn-7Zn, **b** Sn-7Zn-2.5In and **c** Sn-7Zn-0.1Fe-0.1Co solder alloys

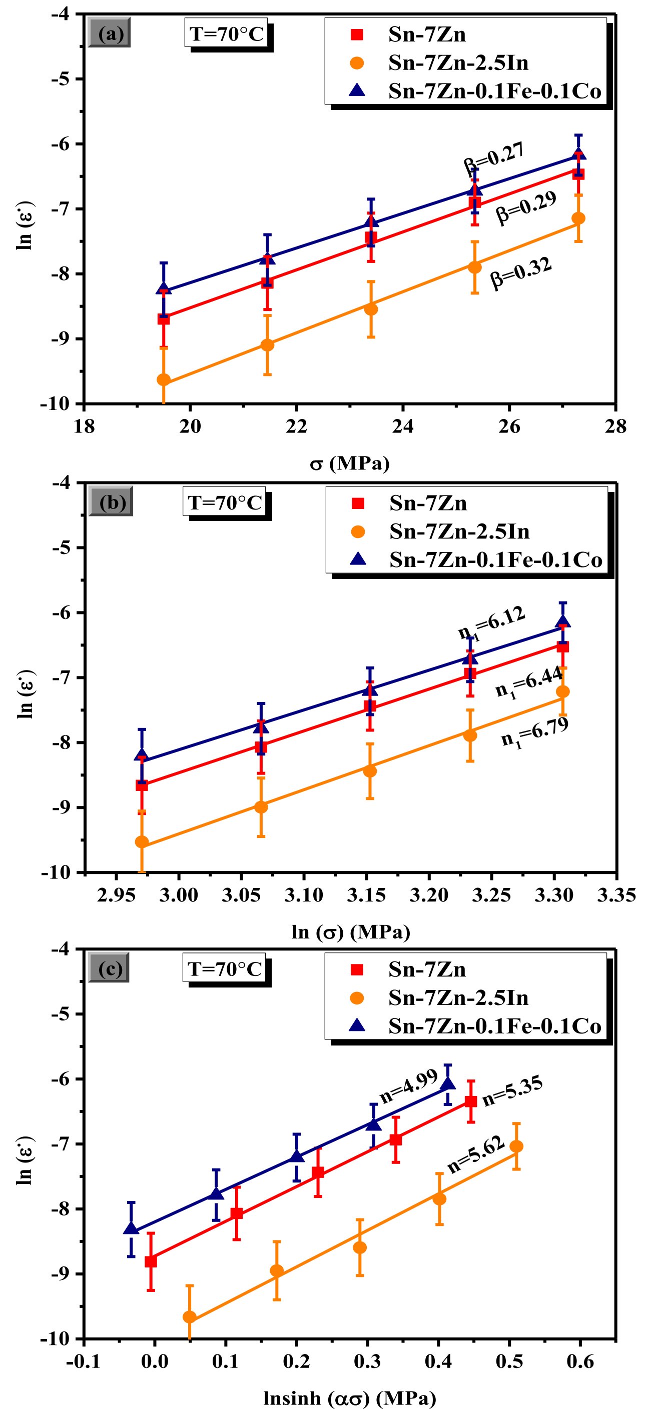

Fig. 12 Determination of β, n_1 and n from the slopes of $\ln \dot{\epsilon} - \sigma$, $\ln \dot{\epsilon} - \ln \sigma$ and $\ln \dot{\epsilon} - \ln [\sinh(\alpha\sigma)]$, respectively, at temperature of T = 70 °C for **a** Sn-7Zn, **b** Sn-7Zn-2.5In and **c** Sn-7Zn-0.1Fe-0.1Co solder alloys

and Sn-7Zn-0.1Fe-0.1Co solder alloys are shown in Fig. 15 and Table 2, respectively. Investigations revealed that the longitudinal velocity decreased from 3424.49 ± 13 to 3408.74 ± 13 m/s adding In to the binary Sn-7Zn, but increased from 3424.49 ± 13 to 3878.24 ± 13 m/s when adding Fe and Co to the

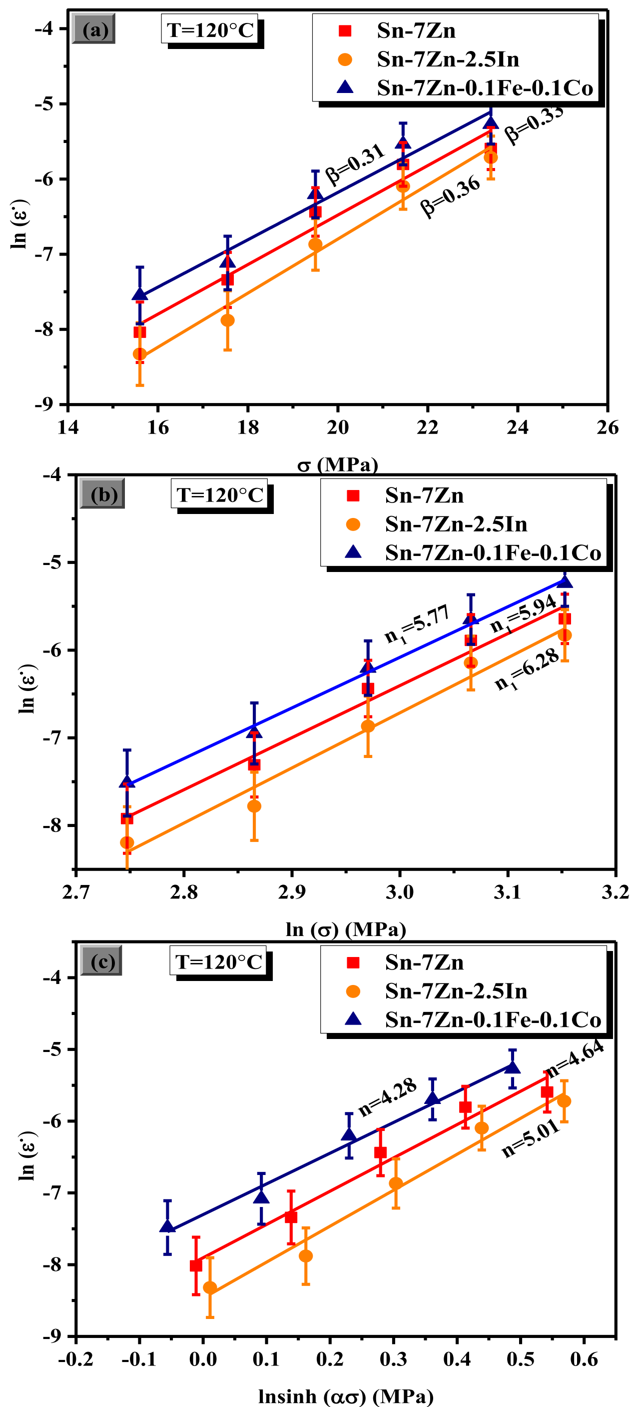

Fig. 13 Determination of β, n_1 and n from the slopes of ln $\dot{\epsilon} - \sigma$, ln $\dot{\epsilon}$ − ln σ and ln $\dot{\epsilon}$ − ln [sinh (ασ)], respectively, at temperature of T = 120 °C for **a** Sn-7Zn, **b** Sn-7Zn-2.5In and **c** Sn-7Zn-0.1Fe-0.1Co solder alloys

binary Sn-7Zn. Furthermore, the In addition to the binary Sn-7Zn increases the shear velocity from 1645.1 ± 8 to 1716.5 ± 8 m/s, while the inclusion of Fe and Co to the binary Sn-7Zn raises the shear velocity value of Sn-7Zn from 1645.1 ± 8 to 1706.2 ± 8 m/s. Interestingly, the longitudinal wave speeds are roughly double the shear wave velocities, which is a notable characteristic of these studies. For the same thickness of the specimen, the transit time of longitudinal wave velocity is around half that of the shear wave velocity. It is also worth noting that the addition of alloying elements has a greater impact on the V_s values than the V_l values, implying that US V_s is a stronger signal for microstructural identification than V_l velocity; similar results were obtained by El-Daly and Hammad [2]. Since the only difference between the examined samples is the formation of IMCs as a result of the addition of In, Fe, and Co, the differences in V_l and V_s values can be attributed to an increased preference for resonance interaction between the US wavefront and IMCs "that behave as robust implications in a soft matrix" and grains. The density of the three specimens was determined using Archimedes' method whose findings are noted in Table 2. The density (ρ) of the alloys fell from 7166.7 ± 5 kg/m^3 to 6956.9 ± 5 kg/m^3 with the In addition to the binary Sn-7Zn and to 6561.1 ± 5 kg/m^3 with the addition of Fe and Co to the plain Sn-7Zn. The presence of a considerable heterogeneous structure in solder alloys, formed during the solidification process as well as the formation of recently obtained IMCs in Sn-7Zn-2.5In and Sn-7Zn-0.1Fe-0.1Co solder alloys, could explain the significant decrease in (ρ) values.

4.3.2 *Impact of alloy addition on Poisson's ratio and elastic moduli*

Both the stress-to-strain proportion, *E*, and the proportion of transverse strain (contraction) to axial strain (elongation) achieved in a uniaxial test, υ, are important factors in technical and engineering implementation. The stiffness of the solid could be indicated using the Young's modulus, where the greater the *E* values, the stiffer the alloy. Conversely, Poisson's ratio, more than any of the other elastic constants, could give more information about how the bonding forces work and how resistant the material is to be shearing and dilatation. Poisson's ratio value is lying between 0 and + 0.5 relying on the compressibility of the alloy. As a result, the smaller the υ is, the more brittle the alloy would become [21, 22]. The obtained experimental data in

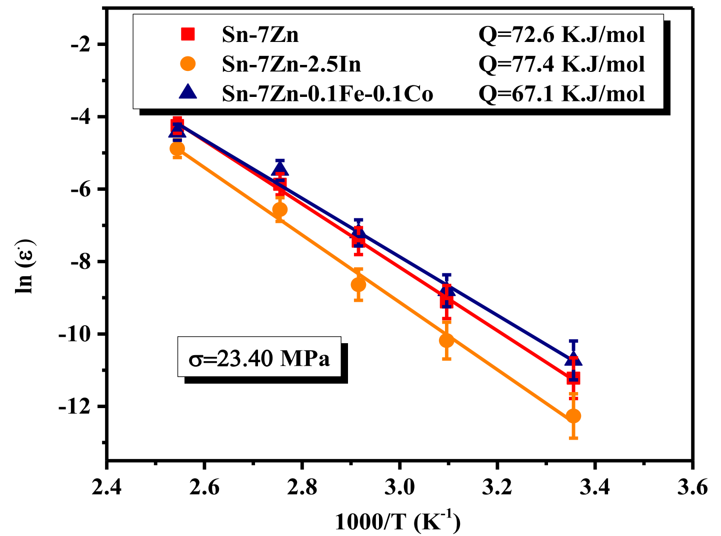

Fig. 14 Temperature dependence of steady-state creep rate and the activation energy (Q) values for Sn-7Zn, Sn-7Zn-2.5In and Sn-7Zn-0.1Fe- 0.1Co solder alloys

Table 1 The Creep-Activation energy (Q), stress exponent (n) and (α) value for Sn-7Zn, Sn-7Zn-2.5In and Sn-7Zn-0.1Fe-0.1Co solder alloys

Alloy	Q (KJ/mol)	Temperature (°C)	α	n
Sn-7Zn		25	0.035	5.83
	72.6	70	0.045	5.35
		120	0.056	4.64
		25	0.037	6.3
Sn-7Zn-2.5In	77.4	70	0.047	5.62
		120	0.057	5.01
		25	0.034	5.48
Sn-7Zn-0.1Fe-0.1Co	67.1	70	0.044	4.99
		120	0.054	4.28

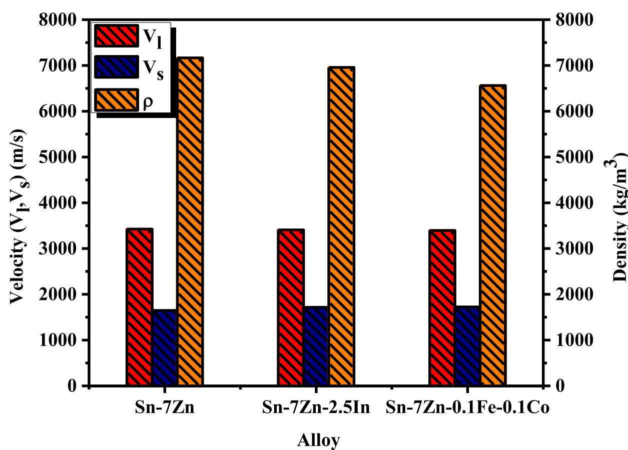

Fig. 15 Ultrasonic wave velocities (longitudinal V_l and shear V_s) and density (ρ) values for Sn-7Zn, Sn-7Zn-2.5In and Sn-7Zn-0.1Fe-0.1Co solder alloys

Table 2 Ultrasonic wave velocities (longitudinal V_l and shear V_s) and density (ρ) values for the given solder alloys without and with application of PMS

Alloy	V_l (m/s)	V_s (m/s)	ρ (Kg/m^3)
Sn-7Zn	3424.49	1645.1	7166.65
Sn-7Zn-2.5In	3408.74	1716.5	6956.89
Sn-7Zn-0.1Fe-0.1Co	3878.24	1706.2	6561.06

this investigation are shown in Fig. 16 and Table 3. The data show that the Poisson's ratio υ decreases from 0.35 to 0.33 with the addition of 2.5In to the binary Sn-7Zn and increases from 0.35 to 0.38 with the addition of 0.1Fe and 0.1Co to the binary Sn-7Zn, demonstrating that Sn-7Zn-0.1Fe-0.1Co exhibits the higher ductility than the investigated samples. Furthermore, the results suggest that the examined alloys have a higher ionic contribution in inter-atomic bonding. In addition, the data in Table 3 and Fig. 16 revealed a variation in Young's modulus' (E) values from 62.6 to 66.7 GPa with In added to the binary Sn-7Zn and from 62.6 to 60.7GPa with 0.1Fe and 0.1Co added to the binary Sn-7Zn. This indicates that the

variation in E values for the three investigated samples is related to the chemical composition of the formed IMCs due to the attributes of ionic bonding force of these compounds.

Furthermore, the K value for Sn-7Zn is found to be 69.6 GPa, while this value is reduced to 65.4 GPa when In was added to the binary Sn-7Zn and raises to 83 GPa when 0.1Fe and 0.1Co were added to the binary Sn-7Zn, implying that Sn-7Zn-0.1Fe-0.1Co has a high compressibility. The elastic constants reduced as the υ values increased, according to the experimental results listed in Table 3. In fact, Liu et al. [22] made similar observations. Zhou et al. [23] proposed an indicator of the scope of the fracture range in metals by empirically linking the plastic characteristics of materials with their elastic moduli by calculating the G/K ratio. In their proposal, the material behaves as either a ductile material if the G/K value is less than 0.374 or as a brittle material if the values exceed 0.571 [23, 24]. The lowest G/K ratio found in this study was 0.23 for Sn-7Zn-0.1Fe-0.1Co, followed by 0.279 for Sn-7Zn, and finally 0.313 for Sn-7Zn-2.5. Because the G/K ratios are all less than 0.374, all the investigated samples act as ductile materials. Even though the previous procedure is overly simplistic, it exposes the ductility tendency of the investigated alloys.

4.3.3 *Impact of alloy addition on the attenuation coefficient (α) and hardness (H)*

The percentage of energy loss suffered by a US plane wave per unit length of a solid specimen, α, is one of the US parameters that must be considered. Attenuation in polycrystalline materials is thought to be primarily caused by the reorientation and diversion of energy (scattering) by precipitates and grains. Thus, how factors like the chemistry of IMCs, the structure, as well as the dimensions, form, kind, and volume fraction of the precipitates affect the scattering that occurs because of the interaction with material deficiency comparable to one wavelength in size can be detected [2]. It is assumed that the incident wave energy can be expected to be reradiated if the IMCs act as oscillators with their own natural frequency. As a result, the scattered wave amplitude and frequency are determined by the damping degree of the oscillator of the surrounding medium. Thus, variations in the value of α should be linked not only to the preceding parameters but also to the homogeneity levels attained by the matrix with the alloying element additions. As shown in Fig. 17 and Table 4, it was discovered that the value of the α for Sn-7Zn is 446.18 ± 57 dB/m, which was reduced to 167.44 ± 57 dB/m with the addition of In to the primary Sn-7Zn solder alloy, and increased to 731.19 ± 57 dB/m with the addition of Fe and Co to the primary Sn-7Zn solder alloy. The highest values of the attenuation coefficient in the Sn-7Zn-0.1Fe-0.1Co solder show that it has a shorter resonant life than the other solders. This could be due to localizing intergranular cracking attached to the formation of IMCs, which allows the vibration cracks spread mechanism. This could be helpful in making new solder alloys by choosing the right components and controlling the attenuation coefficient. The hardness values of the investigated samples are also shown in Fig. 17 and Table 4. It was found that the H value of Sn-7Zn is 2.32 GPa, which is enhanced to 2.84 GPa with doping Sn-7Zn with 2.5In and dropped to 1.76 GPa with the inclusion of Fe and Co to the main Sn-7Zn alloy. The increase in the H values when the IMCs serve as robust implications in the fine matrix could be due to the kind of atomic bonding forces between the components of IMCs and the growth of IMCs volume fraction.

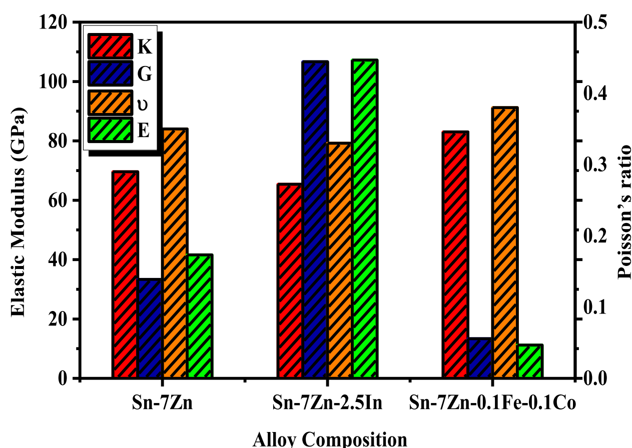

Fig. 16 Elastic modulus: shear modulus (G), bulk modulus (K), Young's modulus (E), and Poisson's ratio (υ) for Sn-7Zn, Sn-7Zn-2.5In, and Sn- 7Zn-0.1Fe-0.1Co solder alloys

5 Conclusion

The effects of the addition of minor quantities of In, Fe, and Co on the microstructure, creep properties, "plastic deformation," and elastic constants of the

Table 3 Experimental values of shear modulus (*G*), bulk modulus (*K*), G/K ratio, Young's modulus, and Poisson's ratio (υ)

Alloy	G (GPa)	K (GPa)	G/K	E (GPa)	υ
Sn-7Zn	19.4 ± 0.1	69.6 ± 0.3	0.279	62.6 ± 0.1	0.35 ± 0.008
Sn-7Zn-2.5In	20.5 ± 0.1	65.4 ± 0.3	0.313	66.7 ± 0.1	0.33 ± 0.008
Sn-7Zn-0.1Fe-0.1Co	19.1 ± 0.1	83 ± 0.3	0.23	60.7 ± 0.1	0.38 ± 0.008

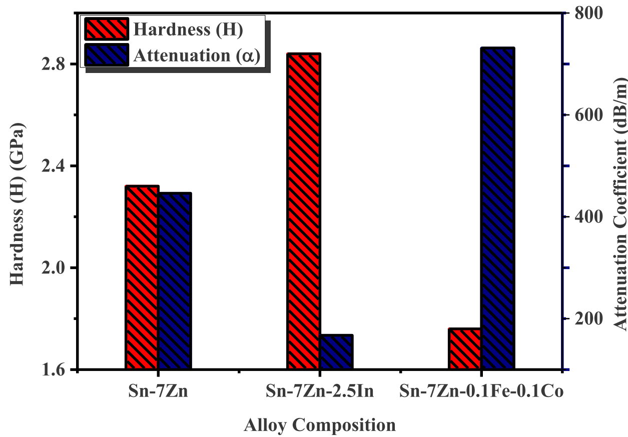

Fig. 17 Hardness (*H*) and attenuation coefficient (α) values for Sn-7Zn, Sn-7Zn-2.5In and Sn-7Zn-0.1Fe-0.1Co

Table 4 Hardness (*H*) and attenuation coefficient (α) values for Sn-7Zn, Sn-7Zn-2.5In and Sn-7Zn-0.1Fe-0.1Co

Alloy	H (GPa)	α (dB/m)
Sn-7Zn	2.32 ± 0.007	446.18 ± 57
Sn-7Zn-2.5In	2.84 ± 0.007	167.44 ± 57
Sn-7Zn-0.1Fe-0.1Co	1.76 ± 0.007	731.19 ± 57

hypo-eutectic Sn-7Zn alloy were studied. The following are the prime conclusions based on the experimental results:

1. From OM and XRD analyses, the addition of 2.5%wt In results in the creation of a new γ-$InSn_4$ IMC distributed in the eutectic region and refine the needle-like Zn phases, whereas the addition of dual 0.1%wt Fe and 0.1%Co into the binary Sn-7Zn alloy changes the microstructure significantly by forming new coarsening γ-$Zn_{21}Co_5$, γ-Co_2Sn_2Zn, and α-$Fe_{0.92}Sn_{0.08}$ IMCs.
2. Mechanical tests demonstrated that the Sn-7Zn-2.5In alloy had significantly lower steady-state creep rate and fracture time than the binary Sn-7Zn. The size, shape, and distribution of γ-$InSn_4$ IMC in the Sn-7Zn-2.5In eutectic regions, however, enhance both strength and ductility. This implies that the Sn-7Zn-2.5In is a visco-plastic material, whereas coarsening IMCs formed due to Fe and Co additions to the Sn-7Zn that reduces the strengthen effects.
3. The activation energies of the Sn-7Zn alloy were 72.6 kJ/mol, 77.4 kJ/mol for the Sn-7Zn-2.5In, and 67.1 kJ/mol for the Sn-7Zn-0.1Fe-0.1Co. This shows that the deformation mechanism transformed from pipe to lattice self-diffusion mechanism for Sn-7Zn-2.5In, while both binary Sn-7Zn and quaternary Sn-7Zn-0.1Fe-0.1Co are controlled by a pipe diffusion mechanism.
4. The elastic modulus is linked to the creation of new IMC phases. The Sn-7Zn-2.5In solder was found to be the most favorable due to a better mix of strength and ductility than the other three alloys.
5. The Poisson's ratio values decreased from 0.35 for Sn-7Zn to 0.33 for In microalloying and 0.38 for Fe and Co microalloying, indicating that the Poisson's ratio reduces as the elastic modulus values increase.
6. Most manufacturing difficulties can be solved by using the right components and a good control technique.

Author contributions

AMET contributed to supervision, conceptualization, methodology, review. SAM contributed to supervision, conceptualization, methodology, project administration, review. IHL contributed to investigation, data curation, software, conceptualization, methodology, validation, resources, writing—original draft, writing—review and editing.

Funding

Open access funding provided by The Science, Technology & Innovation Funding Authority (STDF) in cooperation with The Egyptian Knowledge Bank (EKB). The authors declare that no funds, grants, or other support were received during the preparation of this manuscript.

Data availability

Raw data were generated at Physics department—Faculty of Science—Zagazig University. Derived data supporting the findings of this study are available from the corresponding author upon request.

Declarations

Conflict of interest They have no known competing financial interests or personal relationships that could have appeared to influence the work reported in this paper.

Research involving in human and animal participants This article does not contain any studies involving human participants performed by any of the authors. This article does not contain any studies involving animals performed by any of the authors.

Open Access This article is licensed under a Creative Commons Attribution 4.0 International License, which permits use, sharing, adaptation, distribution and reproduction in any medium or format, as long as you give appropriate credit to the original author(s) and the source, provide a link to the Creative Commons licence, and indicate if changes were made. The images or other third party material in this article are included in the article's Creative Commons licence, unless indicated otherwise in a credit line to the material. If material is not included in the article's Creative Commons licence and your intended use is not permitted by statutory regulation or exceeds the permitted use, you will need to obtain permission directly from the copyright holder. To view a copy of this licence, visit http://creativecommons.org/licenses/by/4.0/.

References

1. A.A. El-Daly, A.A. Ibrahiem, A.E. Hammad, Impact of permanent magnet stirring on dendrite growth and elastic properties of Sn-Bi alloys revealed by pulse echo overlap method. J. Alloys Compd. **767**, 464–473 (2018)
2. A.A. El-Daly, A.E. Hammad, Elastic properties and thermal behavior of Sn-Zn based lead-free solder alloys. J. Alloys Compd. **505**, 798–800 (2010)
3. T. Luan, W. Guo, S. Yang, Z. Ma, J. He, J. Yan, Effect of intermetallic compound on mechanical properties of copper joints ultrasonic-soldered with Sn-Zn alloy. J. Mater. Process. Tech. **248**, 123–129 (2017)
4. J. Jiang, J.E. Lee, K.S. Kim, K. Suganuma, Oxidation behavior of Sn-Zn solders under high-temperature and high-humidity conditions. J. Alloys Compd. **462**, 244–251 (2008)
5. X. Wei, H. Huang, X. Liu, On the advantages of using a hypoeutectic Sn-Zn as lead-free solder material. J. Mater. Lett. **61**, 655–658 (2007)
6. A.A. El-Daly, A.E. Hammad, G.A. Al-Ganainy, A.A. Ibrahiem, Enhancing mechanical response of hypoeutectic Sn-6.5Zn solder alloy using Ni and Sb additions. J. Mater. Des. **52**, 966–973 (2013)
7. Y. Peng, C. Li, K. Xiao, J. Yang, C. Pa, P. Gao, S. Guo, J. Zhang, J. Yi, Effects of Ga alloying on microstructure and comprehensive performances of Sn-9Zn-2Bi alloys for microelectronics industry. J. Micro Electron. Reli. **135**, 114599 (2022)
8. R. Mahmudi, A.R. Geranmayeh, H. Khanbareh, N. Jahangiri, Indentation creep of lead-free Sn-9Zn and Sn-8Zn-3Bi solder alloys. J. Mater. Des. **30**, 574–580 (2009)
9. S. Tikale, M. Sona, K.N. Prabhu, Wettability and bond shear strength of Sn-9Zn lead-free solder alloy reflowed on copper substrate. J. Mater. Sci. Forum **830–831**, 215–218 (2015)
10. A.A. El-Daly, W.M. Desoky, A.F. Saad, N.A. Mansor, E.H. Lotfy, H.M. Abd-El-Moniem, H. Hashem, The effect of undercooling on the microstructure and tensile properties of hypoeutectic Sn-6.5Zn-xCu Pb-free solder. J. Mater. Des. **80**, 152–162 (2015)
11. G. Saad, S.A. Fayek, A. Fawzy, H.N. Soliman, Gh. Mohammed, Deformation characteristics of Al-4043 Alloy. J. Mater. Sci. Eng. A **527**, 904–910 (2010)
12. A.A. El-Daly, F. El-Tantawy, A.E. Hammad, M.S. Gaafar, E.H. El-Mossalamy, A.A. Al-Ghamdi, Structure and elastic properties of eutectic Sn-Cu lead-free solder alloy containing small amount of Ag and In. J. Alloy. Compd. **509**, 7238–7246 (2011)

13. R.M. Shalaby, Effect of indium content and rapid solidification on microhardness and micro-creep of Sn-Zn eutectic lead free solder alloy. J. Cryst. Res. Tech. **45**(4), 427–432 (2010)
14. H. Giefers, M. Nicole, High pressure X-ray diffraction study of all Fe-Sn intermetallic compounds and one Fe-Sn solid-solution. J. Alloy. Compd. **422**, 132–144 (2006)
15. J. Shou-Li, Z. Jian-Feng, L. Jia-Yuan, W. Ri-Chu, P. Chao-Qun, C. Zhi-Young, Influence of cobalt content on microstructure and corrosion performance of extruded Sn-9Zn solder alloys. J. Cent. South. Univ. **27**, 711–720 (2020)
16. M.M. Abou-Krisha, A.M. Abushoffa, Stripping voltametric, conductance and anodic linear polarization analysis on dissolution of electrodeposited Zinc-Cobalt alloy. Int. J. Electochem. Sci. **2**, 418–432 (2007)
17. Q.K. Zhang, F.Q. Hu, Z.L. Song, Z.F. Zhang, Viscoplastic creep and microstructure evolution of Sn-based lead-free solders at low strain. J. Mater. Sci. Eng. A **701**, 187–195 (2017)
18. S. Wiese, M. Rollig, K.J. Wolter, The effect of sown scaling the dimensions of solder interconnects on their creep properties. J. Micro. Electro. Reli. **48**, 843–850 (2008)
19. A.A. El-Daly, A.M. El-Taher, Evolution of thermal property and creep resistance of Ni and Zn-dopped Sn-2.0Ag-0.5Cu lead-free solders. J. Mater. Des. **51**, 789–796 (2013)
20. R.J. McCabe, M.E. Fine, Creep of Tin Sb-solution-strengthened Tin, and Sb-Sn precipitate-strengthened Tin. J. Metal. Mater. Trans. A **33A**, 1531–1539 (2002)
21. A. Kumar, T. Jayakumar, B. Raj, K.K. Ray, Correlation between ultrasonic shear wave velocity and Poisson's ratio for isotropic solid materials. J. Acta Mater. **51**, 2417–2426 (2003)
22. Y.H. Liu, G. Wang, R.J. Wang, D.Q. Zhao, M.X. Pan, W.H. Wang, Super plastic bulk metallic glasses at room temperature. J. Science **315**, 1385 (2007)
23. W. Zhou, L. Liu, B. Li, P. Wu, Q. Song, Structral, elastic and electronic properties of intermetallic in the Pt-Sn system: a density functional investigation. J. Comput. Mater. Sci. **46**, 921–931 (2009)
24. M. Hichour, D. Rached, M. Rabah, S. Benalia, R. Khenata, F. Semari, Structural and elastic properties of antiperouskites XNBa3 (X=As, Sb) under pressure effect. J. Phys. B: Condes Mater. **404**, 4034–4038 (2009)

Publisher's Note Springer Nature remains neutral with regard to jurisdictional claims in published maps and institutional affiliations.